Dalton Transactions c9dt02440a

We have presented the Graphical Abstract text and image for your article below. This brief summary of your work will appear in the contents pages of the issue in which your article appears.

1

New light on an old debate: does the RCN−$PtCl_2$ bond include any back-donation? RCN←$PtCl_2$ backbonding *vs.* the IR $\nu_{C\equiv N}$ blue-shift dichotomy in organonitriles−platinum(II) complexes. A thorough density functional theory − energy decomposition analysis study

Girolamo Casella,* Célia Fonseca Guerra, Silvia Carlotto, Paolo Sgarbossa, Roberta Bertani and Maurizio Casarin

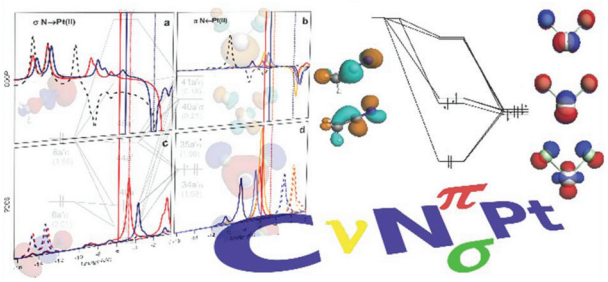

DFT bond and Energy Decomposition Analysis allowed disentangling of the RCN←Pt^{II} π back-donation *vs.* $\nu_{C\equiv N}$ blue-shift dichotomy in organonitrile−platinum(II) complexes. The occurrence of the π back-donation has been ultimately assessed and it causes a lowering of the $\nu_{C\equiv N}$ blue-shift without overwhelming it.

Q3

Please check this proof carefully. Our staff will not read it in detail after you have returned it.

Please send your corrections either as a copy of the proof PDF with electronic notes attached or as a list of corrections. **Do not edit the text within the PDF or send a revised manuscript** as we will not be able to apply your corrections. Corrections at this stage should be minor and not involve extensive changes.

Proof corrections must be returned as a single set of corrections, approved by all co-authors. No further corrections can be made after you have submitted your proof corrections as we will publish your article online as soon as possible after they are received.

Please ensure that:

- The spelling and format of all author names and affiliations are checked carefully. You can check how we have identified the authors' first and last names in the researcher information table on the next page. **Names will be indexed and cited as shown on the proof, so these must be correct.**
- Any funding bodies have been acknowledged appropriately and included both in the paper and in the funder information table on the next page.
- All of the editor's queries are answered.
- Any necessary attachments, such as updated images or ESI files, are provided.

Translation errors can occur during conversion to typesetting systems so you need to read the whole proof. In particular please check tables, equations, numerical data, figures and graphics, and references carefully.

Please return your **final** corrections, where possible within **48 hours** of receipt, by e-mail to: dalton@rsc.org. If you require more time, please notify us by email.

Funding information

Providing accurate funding information will enable us to help you comply with your funders' reporting mandates. Clear acknowledgement of funder support is an important consideration in funding evaluation and can increase your chances of securing funding in the future.

We work closely with Crossref to make your research discoverable through the Funding Data search tool (http://search.crossref.org/funding). Funding Data provides a reliable way to track the impact of the work that funders support. Accurate funder information will also help us (i) identify articles that are mandated to be deposited in **PubMed Central (PMC)** and deposit these on your behalf, and (ii) identify articles funded as part of the **CHORUS** initiative and display the Accepted Manuscript on our web site after an embargo period of 12 months.

Further information can be found on our webpage (http://rsc.li/funding-info).

What we do with funding information

We have combined the information you gave us on submission with the information in your acknowledgements. This will help ensure the funding information is as complete as possible and matches funders listed in the Crossref Funder Registry.

If a funding organisation you included in your acknowledgements or on submission of your article is not currently listed in the registry it will not appear in the table on this page. We can only deposit data if funders are already listed in the Crossref Funder Registry, but we will pass all funding information on to Crossref so that additional funders can be included in future.

Please check your funding information

The table below contains the information we will share with Crossref so that your article can be found *via* the Funding Data search tool. **Please check that the funder names and grant numbers in the table are correct and indicate if any changes are necessary to the Acknowledgements text.**

Funder name	Funder's main country of origin	Funder ID (for RSC use only)	Award/grant number
Università degli Studi di Padova	Italy	501100003500	P-DISC #CARL-SID17 BIRD2017-UNIPD project CHIRoN

Researcher information

Please check that the researcher information in the table below is correct, including the spelling and formatting of all author names, and that the authors' first, middle and last names have been correctly identified. **Names will be indexed and cited as shown on the proof, so these must be correct.**

If any authors have ORCID or ResearcherID details that are not listed below, please provide these with your proof corrections. Please ensure that the ORCID and ResearcherID details listed below have been assigned to the correct author. Authors should have their own unique ORCID iD and should not use another researcher's, as errors will delay publication.

Please also update your account on our online manuscript submission system to add your ORCID details, which will then be automatically included in all future submissions. See here for step-by-step instructions and more information on author identifiers.

First (given) and middle name(s)	Last (family) name(s)	ResearcherID	ORCID iD
Girolamo	Casella	V-9532-2017	0000-0002-8471-0848
Célia	Fonseca Guerra	E-8851-2011	0000-0002-2973-5321
Silvia	Carlotto		0000-0003-0043-3538
Paolo	Sgarbossa		
Roberta	Bertani		
Maurizio	Casarin		0000-0002-3347-8751

Queries for the attention of the authors

Journal: **Dalton Transactions** Paper: **c9dt02440a**

Title: **New light on an old debate: does the RCN–$PtCl_2$ bond include any back-donation? RCN←$PtCl_2$ back-bonding *vs.* the IR $\nu_{C\equiv N}$ blue-shift dichotomy in organonitriles–platinum(II) complexes. A thorough density functional theory – energy decomposition analysis study**

For your information: You can cite this article before you receive notification of the page numbers by using the following format: (authors), Dalton Trans., (year), DOI: 10.1039/c9dt02440a.

Editor's queries are marked like this Q1, Q2, and for your convenience line numbers are indicated like this 5, 10, 15, ...

Please ensure that all queries are answered when returning your proof corrections so that publication of your article is not delayed.

Query Reference	Query	Remarks
Q1	Please confirm that the spelling and format of all author names is correct. Names will be indexed and cited as shown on the proof, so these must be correct. No late corrections can be made.	
Q2	Do you wish to add an e-mail address for the corresponding author? If so, please provide the relevant information.	
Q3	The Graphical Abstract text currently exceeds the space available for the published version. Please trim the text so that it is shorter than 250 characters (including spaces).	
Q4	The meaning of the sentence beginning "Results for all ..." is not clear - please provide alternative text.	
Q5	The meaning of the sentence beginning "Moreover, the virtual ..." is not clear - please provide alternative text.	
Q6	Text has been provided for footnotes a and b in Table 3, but there do not appear to be corresponding citations in the table. Please indicate suitable locations for the footnote citations.	
Q7	The meaning of the sentence beginning "In addition, by the ..." is not clear - please provide alternative text.	
Q8	The meaning of the phrase "which effects should both to cause" in the sentence beginning "In general, this ..."is not clear - please provide alternative text.	
Q9	The meaning of the phrase "with respect to free ligands ones" in the sentence beginning "This causes lower ..." is not clear - please provide alternative text.	
Q10	The meaning of the phrase "resulted more polarized going from" in the sentence beginning "For the purely ..." is not clear - please provide alternative text.	
Q11	The meaning of the sentence beginning "The role of the ..." is not clear - please provide alternative text.	

Q12	The meaning of the sentence beginning “These results ruled ...” is not clear - please provide alternative text.	
Q13	Ref. 6*b*: Please provide the journal title.	
Q14	Please indicate where ref. 19 should be cited in the text.	

Dalton Transactions

PAPER

New light on an old debate: does the RCN–$PtCl_2$ bond include any back-donation? RCN←$PtCl_2$ backbonding *vs.* the IR $\nu_{C\equiv N}$ blue-shift dichotomy in organonitriles–platinum(II) complexes. A thorough density functional theory – energy decomposition analysis study†‡

Cite this: DOI: 10.1039/c9dt02440a

Girolamo Casella, *§[a,b] Célia Fonseca Guerra,[c,d] Silvia Carlotto,[e] Paolo Sgarbossa,[f] Roberta Bertani[f] and Maurizio Casarin[e]

Received 8th June 2019,
Accepted 31st July 2019

DOI: 10.1039/c9dt02440a

rsc.li/dalton

For a series of organonitrile [RCN (R = Me, CF_3, Ph, CH_3Ph, CF_3Ph)] ligands, the nature of the N–Pt bond in the related *cis*-/*trans*-$(RCN)_2PtCl_2$ complexes has been computationally investigated by Density Functional Theory. A fragment based bond analysis has been performed in the canonical Kohn–Sham molecular orbitals framework, and it has been ultimately assessed that this bond is characterized both by N→Pt σ and by N←Pt π contributions. Voronoi Deformation Density charges further confirms the occurrence of N←Pt π interactions. Moreover, the Energy Decomposition Analysis-Natural Orbital for Chemical Valence (EDA-NOCV) method shows that the strength of the N←Pt π interaction is not negligible by contributing to about 30–40% of the total orbital interaction. Finally, the well-known $\nu_{C\equiv N}$ blue-shift occurring upon coordination to Pt^{II}, has been thoroughly investigated by exploiting the EDA-NOCV and by evaluating $\nu_{C\equiv N}$ and force constants. The origin of the $\nu_{C\equiv N}$ blue-shift in these systems has been discussed on the basis of the CN bond polarization. N←Pt π backbonding causes only a systematic decrease of the observed $\nu_{C\equiv N}$ blue-shift when compared to the one calculated for RCN–X (X = H^+, alkaline, earth-alkaline and transition metal ions, Lewis acids) herein reported (X = purely σ acceptors.

Introduction

Organonitrile ligands (RCN) are a class of reactants used to synthesize important compounds, by means of nucleophilic and electrophilic additions as well as dipolar cyclo-addition, either for laboratory or for industrial applications.[1–6] A well-known drawback of the organonitriles' chemistry lies in their inertness as free ligands, and the enhancement of their reactivity is still one of the most pursued goals, by means of both theoretical and experimental approaches.[1–3,6–10] Despite the choice of suitable R groups contributing to activate the C≡N triple bond, greater activation may be achieved through the formation of organonitrile complexes with suitable transition metals (TMs).[1–3] Incidentally, both approaches may be exploited at the same time, thus organonitriles' reactivity may benefit both contributions.

As a rule, both strong electron-acceptor R groups and/or TMs in relatively high oxidation states contribute to improving nucleophilic or dipolar cyclo-addition reactions, while, *e.g.*, electron rich, low oxidation state TMs may favor electrophilic substitutions.[1–3]

[a]*Dipartimento di Scienze della Terra e del Mare, Università degli Studi di Palermo, Via Archirafi, 22, 90123 Palermo, Italy*
[b]*Consorzio Interuniversitario di Ricerca in Chimica dei Metalli nei Sistemi Biologici (C.I.R.C.M.S.B.) – Piazza Umberto I, 70121 Bari, Italy*
[c]*Department of Theoretical Chemistry and Amsterdam Center for Multiscale Modeling, Vrije Universiteit Amsterdam, De Boelelaan 1083, 1081 HV Amsterdam, The Netherlands*
[d]*Leiden Institute of Chemistry, Gorlaeus Laboratories, Leiden University, Einsteinweg 55, 2333 CC Leiden, The Netherlands*
[e]*Dipartimento di Scienze Chimiche, Università degli Studi di Padova, via F. Marzolo 1, 35131 Padova, Italy*
[f]*Dipartimento di Ingegneria Industriale, Università degli Studi di Padova, via F. Marzolo 9, 35131 Padova, Italy*

†We wish to dedicate this work to the memory of Prof. Rino A. Michelin and his enduring human and scientific legacy.

‡Electronic supplementary information (ESI) available. See DOI: 10.1039/c9dt02440a

§G. C. made this work during his leave of absence period at the Prof. Maurizio Casarin research group at the Università degli Studi di Padova.

Concerning organonitrile–Pt^{II} complexes (RCN–Pt^{II}), Density Functional Theory (DFT) theoretical studies have proven to be a useful tool for nucleophilic, electrophilic and cyclo-addition reactions, allowing not only the distinction between kinetic and thermodynamic effects, but also their quantitative estimation.[7–9] However, the roles and contributions of R groups and TMs' centers on the reactivity of organonitriles cannot be sometimes simply explained as the straight result of heuristic considerations; in fact, the same contributions, *e.g.*, metal size or charge, R group, *etc.*, may differently affect the final reaction outcome of similar RCN–Pt^{II} intermediates, mainly due to mechanistic issues.[3,8]

In general, numerical experiments confirmed how the increased reactivity of coordinated organonitriles matches well with the energy position of the relevant Highest Occupied Molecular Orbital (HOMO) and the Lowest Unoccupied Molecular Orbital (LUMO) in the corresponding Pt(II) complexes.[2,7,8] As such, it is well known that, after coordination, the LUMO of the organonitriles is lowered in energy, causing an increase in RCNs' Lewis acidity while, in some cases, the HOMO may increase its energy, thus increasing the Lewis basicity of the coordinated ligands.[2,8,11]

Infra-Red (IR) spectroscopy has been always a valuable tool in organonitrile chemistry to assess some structural and reactivity properties of coordinated RCN–X nitriles (X = transition metals, alkali, and alkaline earth cations, BF_3, BCl_3, H^+). Besides to give proof of the N–X bond formation, observation of the $\nu_{C\equiv N}$ blue (red)-shift, also indicates that the coordinated nitriles can be subjected to nucleophilic(electrophilic) addition reactions.[1]

The occurrence of the $\nu_{C\equiv N}$ blue(red)-shift in coordinated organonitriles has been rationalized in terms of the competitive effects arising from the σ/π donation/backdonation, which in turn causes a decrease/increase of the antibonding σ*/π* CN orbitals' population, respectively.[1,3,24]

An old debate about RCN–Pt^{II} complexes concerns the experimental proof of the N–Pt^{II} bond formation after the synthesis of the desired RCN–Pt^{II} intermediate. It is well known that the C≡N vibrational ($\nu_{C\equiv N}$) frequency experiences a hypsochromic shift (blue-shift) upon the coordination of RCN to Pt^{II}.[12–14]

Moreover, the $\nu_{C\equiv N}$ blue-shift has been observed, and confirmed computationally[14–18] with results pointing to the leading role played by the force constant ($k_{C\equiv N}$) increasing also for several RCN–X (X = transition metals, alkali, and alkaline earth cations, BF_3, BCl_3, H^+) species.[15–18]

The explanation of this behavior based solely on the σ/π donation/backdonation orbital interaction model discussed earlier, would imply the lack of any N←Pt π back-donation, or at least the occurrence of such interaction which cannot overcome the effect of the N→Pt σ donation.[1]

To the best of our knowledge few computational studies on the nature of the N–Pt interaction have been reported so far. Concerning the N–Pt^0 bond, for systems with NH_3[20] or N-heterocyclic carbene ligands (NHC),[21] the occurrence of a non-negligible N←Pt^0 π back-donation has been systematically reported. Conversely, for bis-acetonitrile(-benzonitrile)–$Pt^{II}Cl_2$ complexes, theoretical studies on the nature of the N–Pt^{II} chemical bond always pointed to the lack, or to a very poor π-acceptor capability, of nitrile ligands.[14a,22–24] Indeed, this behavior seems to be in line with the poor accepting electron density capability of organonitrile ligands with respect to other unsaturated common ligands, such as CNR or CO.[24]

Nonetheless, the π-acceptor capability of these ligands has been only qualitatively inferred so far by topological investigations of the electronic density distribution, charge decomposition analysis,[22–24] and composition and overlap intensities of the molecular orbitals involved in the N–Pt^{II} bond.[14a]

On these grounds, we deemed: (i) to deeply investigate, by combining the DFT bond analysis in the canonical Kohn–Sham Molecular Orbitals (KS-MO) framework, Voronoi Density Deformation (VDD)[25] charges, combined Energy Decomposition Analysis[26–29] and Extended Transition State-Natural Orbital for Chemical Valence[30,31] (from now on EDA-NOCV) methods, the nature and the strength of the interactions characterizing the N–Pt^{II} bond, to get a definitive quantitative picture of the bonding interactions, and (ii) to study the ensuing effects on the C≡N bond upon coordination, in order to shed ultimate light on the aforementioned discussed N←Pt π back-donation *vs.* $\nu_{C\equiv N}$ blue shift dichotomy.

In the forthcoming discussion, a series of Pt^{II} complexes with acetonitrile (ACN) and benzonitrile (PhCN), already characterized experimentally,[14] and some analogous substituted model ligands, namely: trifluoroacetonitrile (CF_3CN), 4-methylbenzonitrile (*p*-tolunitrile: *p*-TOL) and 4-(trifluoromethyl)benzonitrile (*p*-TFM) (see Fig. 1) will be tackled to investigate the potential role of the substituents R on the N–Pt^{II} bond as well as their potential effect on the C≡N bond.

Results and discussion

Coordination thermodynamics

A first insight into the nature of the Pt–N bond for the models herein considered was obtained by evaluation of the relevant coordination thermodynamics. Theoretical thermodynamic data related to the formation of complexes at standard conditions in the gas phase, and evaluated according to the Scheme (a) (see Computational methods section), are collected in Table 1. Interestingly, irrespective of the *cis*/*trans* pairs considered, the corresponding $\Delta\Delta G^\circ$ values at 298 K are systemati-

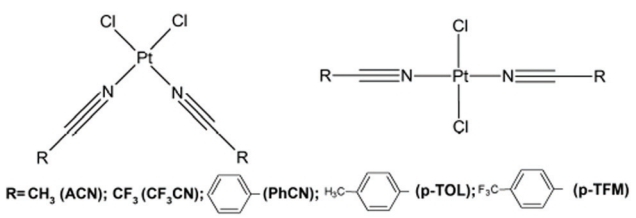

Fig. 1 Schematic representation of the *cis* and *trans* isomers of the complexes herein investigated. (Abbreviations in parentheses.) The list of abbreviations and complexes numbering is given in the Computational details section.

Table 1 Calculated thermodynamic data (kcal mol^{-1}) for the studied complexes in gas phase at 298.15 K and 1 atm. Data calculated at 273.15 K and 1 atm are given in parentheses

	ΔH°	$T\Delta S^\circ$	ΔG°
***cis*-1**	−71.3 (−71.7)	−20.0 (−17.2)	−51.3 (−54.5)
***cis*-2**	−65.8 (−66.3)	−22.1 (−20.5)	−43.7 (−45.8)
***cis*-3**	−73.8 (−73.9)	−22.7 (−20.9)	−51.1 (−53.0)
***cis*-4**	−74.2 (−74.4)	−22.8 (−21.1)	−51.4 (−53.3)
***cis*-5**	−72.6 (−72.7)	−23.8 (−21.2)	−48.8 (−51.5)
***trans*-1**	−76.4 (−76.5)	−19.6 (−16.1)	−56.8 (−60.4)
***trans*-2**	−70.6 (−70.5)	−20.2 (−18.3)	−50.4 (−52.2)
***trans*-3**	−77.8 (−78.0)	−20.6 (−18.6)	−57.2 (−59.6)
***trans*-4**	−78.5 (−77.7)	−20.5 (−16.3)	−58.0 (−61.4)
***trans*-5**	−76.9 (−77.0)	−21.6 (−19.4)	−55.3 (−57.6)

cally almost the same, *ca.* 6–7 kcal mol^{-1}. A further point to be stressed, except for the fluorinated complexes, is the close similarity of the ΔG° values along a specific series (*cis* or *trans*), which is consistent with a quite similar bonding interaction. To look into the temperature effects on the thermodynamic stability of Pt^{II} complexes, a further series of numerical experiments at 273.15 K were also carried out. Differences between ΔG° and $\Delta G^{273.15}$ values differ by no more than 4 kcal mol^{-1} (see Table 1). These differences have ultimately to be traced back to the entropic term (Table 1).

Electronic structure and bonding analysis

According to the frontier orbitals molecular approach, it is well known that the ligand HOMO and LUMO energies (E^{HOMO} and E^{LUMO}, respectively) play some role in determining the RCN reactivity;[7–9,32,33] in particular, a lower RCN E^{LUMO} points to a higher reactivity towards nucleophilic addition.¶

In this regard, two distinct strategies may be adopted to tune the RCN E^{LUMO}: (i) to exploit the electron-withdrawing (releasing) properties of suitable R groups (the electron-withdrawing CF_3 group in CF_3CN and *p*-TFM induces a sizable E^{LUMO} decreasing with respect to the parents ACN and PhCN, while the electron-releasing CH_3 group in *p*-TOL causes a E^{LUMO} increase, see Table 2); (ii) to take advantage of the coordination of the ligand to a metal center (a systematic energy lowering of MOs reminiscent of the free ligands' LUMO accompanies the formation of the complexes, see Table 2). A thorough charge density analysis of the *cis*-/*trans*-Cl_2Pt–NCR MOs reminiscent of the free ligands' LUMO indicates minor contributions from Pt-based atomic orbitals (AOs) (see Table 2).‖ Moreover, the inspection of this table testifies that the effect of the substituents on E^{LUMO} is larger for the ACN derivatives when compared to that for the PhCN ones. As such,

¶Along the investigated series, both HOMO and LUMO correspond to π orbitals mainly localized on the CN group; the former (latter) is bonding (antibonding) in nature with respect to the C≡N interaction.

‖In all the PhCN-based complexes, the MOs reminiscent of the free ligands' LUMO correspond to the complex LUMO as well; at variance to that, in ACN-based complexes, the MOs reminiscent of the free ligands' LUMO correspond to the complex LUMO+1. It has to be noted that LUMO and LUMO+1 in the ACN-based complexes are very close in energy.

Table 2 LUMO (L) and HOMO (H) energies (eV) of free ligands and the corresponding reminiscent MOs on the complexes. (Orbitals' localization of reminiscent ligands' MOs, and the corresponding contribution % of the ligands' fragments to the complex MOs are given in brackets and parentheses, respectively)

	L	H
ACN	−0.40	−8.14
***cis*-1**	−1.64 [+1] (83%)	−7.48 [−7] (13%)
***trans*-1**	−1.89 [+1] (87%)	−7.35 [−7] (17%)
CF_3CN	−2.27	−9.73
***cis*-2**	−3.38 [+1] (82%)	8.78 [−7] (9%)
***trans*-2**	8.78 [−7] (9%)	−8.70 [−8] (15%)
PhCN	−2.60	−6.89
***cis*-3**	−3.13 [0] (93%)	−6.95 [−5] (31%)
***trans*-3**	−3.13 [0] (95%)	−6.77 [−6] (33%)
***p*-TOL**	−2.43	−6.57
***cis*-4**	−2.94 [0] (94%)	−6.69 [−5] (35%)
***trans*-4**	−2.93 [0] (95%)	−6.50 [−6] (36%)
***p*-TFM**	−3.24	−7.39
***cis*-5**	−3.74 [0] (94%)	−7.38 [−5] (30%)
***trans*-5**	−3.76 [0] (96%)	−7.23 [−6] (31%)

the homologous ACN/CF_3CN and TOL/TFM free ligand pairs are particularly enlightening; the ΔE^{LUMO} between ACN and CF_3CN is ∼1.90 eV, and it reduces to ∼0.81 eV when we move from TOL to TFM. Nonetheless, it has also to be highlighted that, when considering the absolute E^{LUMO} values, the presence of the aromatic group induces a higher energy decrease. As far as the effect of the coordination to a metal center is concerned, the further E^{LUMO} lowering associated with the complex formation amounts to ∼1.1–1.2 (1.3–1.5) eV for ACN-based *cis* (*trans*) complexes, while such a lowering is ∼0.5 eV for all PhCN-based complexes. Outcomes demonstrated that there is an electrostatic contribution of the metal in the energy lowering of the RCN E^{LUMO}, irrespective of the R group.

All these findings depict a trend in the E^{LUMO} variation, which accounts for the R group, the eventual substituent it carries, and the coordination to the metal.

All these findings depict a trend in the E^{LUMO} variation, which accounts for the R group, the eventual substituent it carries, and the coordination to the metal. Finally, E^{HOMO} seems to play some role in rationalizing the RCN reactivity in the 1,3-dipolar cycloadditions;[32,33] indeed an E^{HOMO} increase should favor the interaction with the polarophile.[7–9,32,33] HOMO and LUMO energies for free and coordinated ligands are reported in Table 2.

Theoretical results herein collected indicate that the R group and its eventual substituents similarly affect E^{HOMO} and E^{LUMO} (see Table 2), while a different trend is found when the coordination to the metal is considered. More specifically, ACN-based ligands show an E^{HOMO} increase upon coordination (∼1.3 eV), while the E^{HOMO} of PhCN-based ligands remains almost unchanged (∼0.1 eV).

N–Pt^{II} bonding scheme

Thermodynamic results showed that the organonitriles' coordination involves quite similar energies in the *cis*/*trans* series, except for some differences observed for the fluorinated

complexes, which can be confidentially ascribed to the strong withdrawing effect of the F atoms. Moreover, data in Table 2 indicate that, besides the R group's effects, RCN to Pt coordination similarly affects the E^{LUMO} lowering: this trend is more evident for the PhCN-based complexes where the effect of the F atoms is buffered by the presence of the phenyl ring. To summarize: the results so far discussed seem to point to a very similar N–Pt^{II} interaction mechanism. Table 2 shows LUMO (L) and HOMO (H) energies (eV) of free ligands and the corresponding reminiscent MOs on the complexes. (Orbitals' localization of reminiscent ligands' MOs, and corresponding contribution % of the ligand fragments to the complex MOs are given in brackets and parentheses, respectively.)

Then, we studied the N–Pt^{II} bonding by exploiting KS-MO and VDD analysis and evaluating the corresponding energies' contributions according to the EDA-NOCV analysis (see the Computational details section).

We will discuss both mono- and di-coordinated models complexes, according to schemes **S1** and **S2** (see the Computational details section). Due to the very high analogies found in the bonding mechanisms for all complexes investigated here, only ACN derivatives will be discussed as paradigms for all systems considered (contour plot and numbering of all orbitals involved for all systems studied are given in Fig. S1 and S2 of the ESI‡).

The plots of the Crystal Orbital Overlap Population (COOP; see the Computational methods section) for ***cis*-1** and ***trans*-1**, are given in Fig. 2 and 3, respectively. They allow for assessing the bonding/antibonding nature of the orbital interactions, according to the corresponding orbitals' overlaps, along with the relevant N→Pt^{II} σ or N←Pt^{II} π type of interaction (see

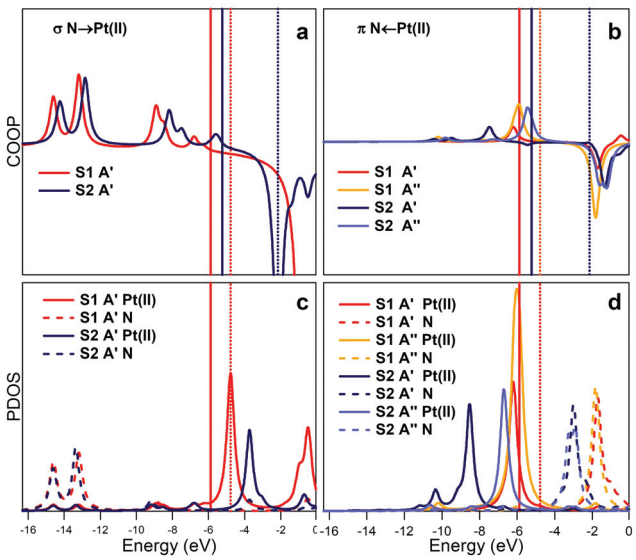

Fig. 2 COOPs for the σ N→Pt^{II} (panel a) and the π N←Pt^{II} (panel b) interactions and relevant PDOS (panels c and d for σ and π, respectively) for ***cis*-1** complex. Vertical solid lines: HOMO; vertical dotted lines: LUMO. [Ordinates' values in arbitrary units. Panels a and b: y = −0.1–0.1; panels c and d: y = 0.0–2.4.]

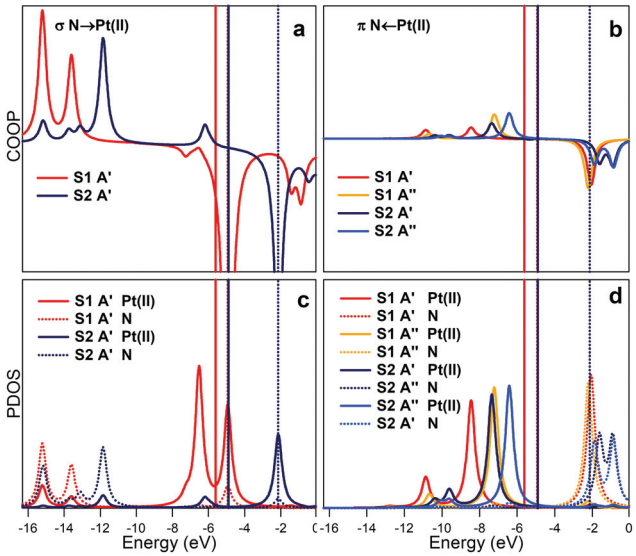

Fig. 3 COOPs for the σ N→Pt^{II} (panel a) and the π N←Pt^{II} (panel b) interactions and relevant PDOS (panels c and d for σ and π, respectively) for ***trans*-1** complex. Vertical solid lines: HOMO; vertical dotted lines: LUMO. [Ordinates' values in arbitrary units. Panels a and b: y = −0.1–0.1; panels c and d: y = 0.0–2.4.]

Table S1 in ESI‡). Results for all the complexes resulted very similar for all the complexes even in the interactions of PhCN derivatives were systematically localized about 1 eV higher than the ACN ones (a comparison of all COOPs is given in Fig. S3 as the ESI‡). The N→Pt^{II} σ and the N←Pt^{II} π interactions, are shown in Fig. 2a and b, respectively, and an overall bonding interaction is highlighted. For both *cis*/*trans* species, the σ N→Pt^{II} interactions (observed only in the A′ irrep) are mainly localized in the −15/−13 eV and −9/−7 eV ranges, while the π N←Pt^{II} interactions, occurring in both A′ and A″ irreducible representations (irreps) are found around −10/−5 eV. Moreover, the corresponding plot of the Partial Density of States (PDOS; see the Computational methods section) for the deepest N→Pt^{II} σ interactions indicates a predominant contribution of the N orbitals of the ligand fragment, while N←Pt^{II} π ones are mainly ascribable to the contribution of Pt orbitals of the *cis*/*trans*-$PtCl_2$ ($^{C,T}PtCl_2$) fragment as well as to the σ interactions localized around −9/−7 eV. Note the occurrence of an overlap between σ and π interactions, in the A′ irrep, located in the −10/−7 eV range.

Bonding scheme of the mono-coordinated forms of the (*cis*/*trans*)-1 complexes (S1)

The resulting σ and π bonding schemes are given in Fig. 4 and 5 for the mono-coordinated species of ***cis*-1** and ***trans*-1**, respectively. For both mono-coordinated species, the σ bond mechanism is based on the donor–acceptor interaction between the nitrogen lone pair orbital of the ligand with orbitals mainly of Pt 6s character, (namely: 41a′ and 38a′ for the mono-coordinated $^{C,T}PtCl_2$, respectively; see Fig. 4 and 5) and further suitable Pt^{II} valence orbitals depending on the *cis*/*trans* configuration. Particularly, these orbitals mostly correspond to

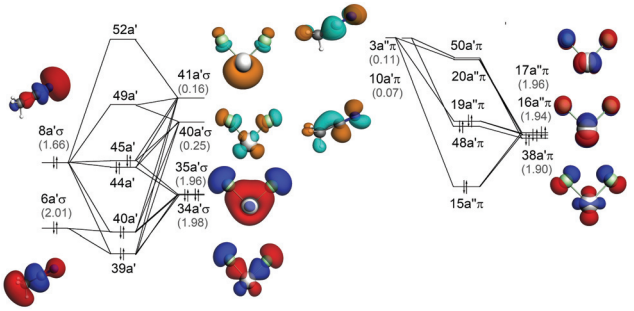

Fig. 4 σ/π bonding scheme for the mono-coordinated model of ***cis*-1**. Orbitals' population is given in parentheses. Isosurface value: 0.05 $e^{1/2}$ $Å^{-3/2}$. (Red-blue phases = occupied orbitals; brown-teal phases = virtual orbitals.) Ligand fragment orbitals are given on the left of each bonding scheme.

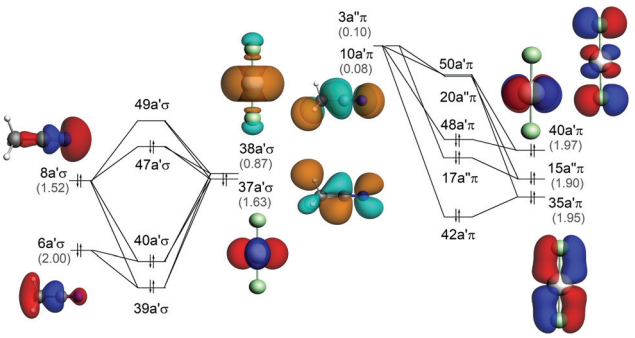

Fig. 5 σ/π bond formation scheme for the mono-coordinated model of ***trans*-1**. Orbitals' population is given in parentheses. Isosurface value: 0.05 $e^{1/2}$ $Å^{-3/2}$. (Red-blue phases = occupied orbitals; brown-teal phases = virtual orbitals.) Ligand fragment orbitals are given on the left of each bonding scheme.

Pt d_{xy} orbitals for ***cis*-1** (40a′ Fig. 4) and Pt $d_{x^2-y^2}$ and d_{z^2} for ***trans*-1** (still localized in 38a′, Fig. 5).

We remind that, as defined in the Computational details section, the $^{T}PtCl_2$ was prepared by properly setting up its molecular electron configuration in order to get a closed-shell fragment and to avoid intra-electronic rearrangements in the fragment. The only electronic configuration satisfying this requirement led to a non-Aufbau occupation where the inner virtual orbital was just the 38a′ one. This is in line with the use of the Pt 6s orbital in the σ bond, analogously to the ***cis*-1** Q5 mono-coordinated species. Moreover, the virtual 38a′ orbital, rise up its energy after coordination.

For $^{T}PtCl_2$, inspection of the orbitals' population in Fig. 5 indicates that the N→Pt^{II} interaction is also characterized by a non-negligible 37a′→38a′ polarization involving $^{T}PtCl_2$, more likely as a consequence of the *ad hoc* electronic configuration used.

Note that a N←Pt^{II} π back-donation has also been obtained.

Bonding scheme of the di-coordinated forms of the (*cis*/*trans*)-1 complexes (S2)

Contrarily to **S1**, no fragment electronic configuration preparation was needed. In this context, for the σ interaction, it is possible to see (Fig. 6 and 7) how bonding schemes for ***cis*-1** and ***trans*-1** involve identical orbitals. Moreover, σ and π interactions, as foreseeable, are analogous to what is observed in **S1**. The N lone pair donates to the same Pt based orbitals of the other fragment. The unique difference with respect to **S1**, for ***cis*-1**, lies in the interaction with only one virtual orbital, which is almost entirely characterized by the combination of the 40a′ (71%) and 41a′ (24%) FMOs involved in **S1**.

For ***trans*-1**, the straight comparison between **S1** and **S2** is flawed by the non-ground state configuration of $^{T}PtCl_2$ in **S1**. Nonetheless, an analogy in the bonding mechanism could also be inferred in this case. After donation to the virtual 38a′ (Fig. 5) and 49a′ (Fig. 7) orbitals, a comparison of 8a′ population, in **S1** (Fig. 5) and **S2** (Fig. 7) shows a significant difference, with the orbital in **S2** being more populated than in **S1**. In addition, also the non-negligible contribution of 37a′ (Fig. 5) and 46a′ (Fig. 7) should be accounted for. Moreover, we should also consider that in **S1** a small 8a′→37a′ population transfer could also occur which could be responsible for the population differences of the 8a′ orbitals in **S1** and **S2**.

To summarize, in both steps considered, all complexes showed that the N–Pt^{II} bond is characterized, as one could

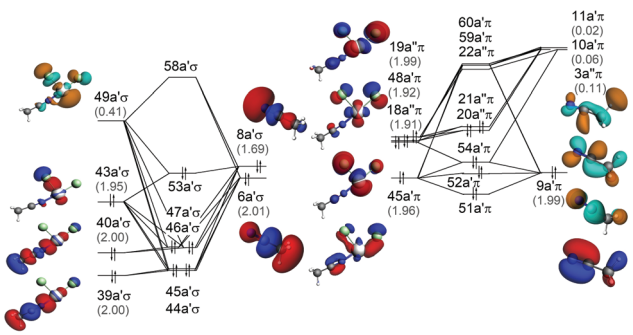

Fig. 6 σ/π bond formation scheme for the di-coordinated model of ***cis*-1**. Orbitals' population is given in parentheses. Isosurface value: 0.05 $e^{1/2}$ $Å^{-3/2}$. (Red-blue phases = occupied orbitals; brown-teal phases = virtual orbitals.) Ligand fragment orbitals are given on the right of each bonding scheme.

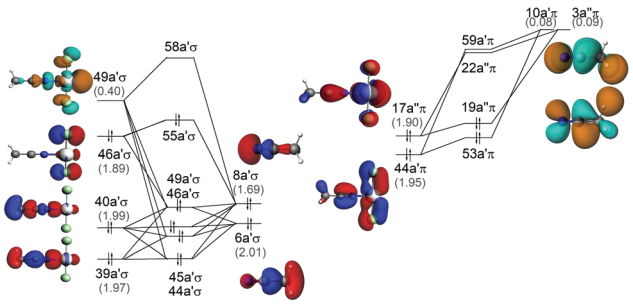

Fig. 7 σ/π bond formation scheme for the di-coordinated model of ***trans*-1**. Orbitals' population is given in parentheses. Isosurface value: 0.05 $e^{1/2}$ $Å^{-3/2}$. (Red-blue phases = occupied orbitals; brown-teal phases = virtual orbitals.) Ligand fragment orbitals are given on the right of each bonding scheme.

expect, by a σ interaction involving the nitrogen long pair and the 6s and suitable 5d Pt^{II} orbitals. Nonetheless, the N←Pt^{II} π back-donation was also observed, characterized by the involvement of anti-bonding π* CN orbitals.

A final remark concerns the N→Pt^{II} and N←Pt^{II} interactions in the A′ irreps. As previously discussed with regard to COOPs (Fig. 2 and 3), an inspection of the composition of the orbitals in this region confirmed a non-negligible admixture of σ and π types for all complexes investigated. For ***cis***/***trans*-1**, this mixing involved mainly the Pt^{II} bases orbitals 38a′ in **S1** (Fig. 4) and 45a′ and 48a′ in **S2** (Fig. 6), these last contributions are not reported in Fig. 4–7 (numbering of the analogous orbitals for all systems is reported in Table S4 as the ESI‡).

VDD charge analysis

By VDD charge (Δ*Q*) analysis, we gained insights into the electron density flow on the atoms of interest after the Cl_2Pt^{II}–NCR bond formation, on both coordination steps so far considered.

Accounting for the very similar behavior of all complexes, also in this case the discussion will be focused on ***cis***/***trans*-1** complexes. Δ*Q* and relevant $\Delta Q^{\Gamma}_{Pauli}$ and ΔQ^{Γ}_{Orb} charges for ***cis*-1** and ***trans*-1** are given in Table 3, while charges for all complexes are given in Tables S2–S5 as the ESI.‡ In Table 3, data for ***trans*-1** in **S1** are not reported due to the non-Aufbau configuration used for the $^{T}PtCl_2$ fragment (see "the Computational methods: VDD analysis" section for the meaning of Δ*Q*, $\Delta Q^{\Gamma}_{Pauli}$ and ΔQ^{Γ}_{Orb} charges).

Concerning the C≡N group, in **S1** and **S2** steps, the N_{CN} shows a small negative charge after the N–Pt^{II} bond formation, which is mainly ascribable to the π A″ term. The inspection of the relevant $\Delta Q^{A''}_{Pauli}$ and $\Delta Q^{A''}_{Orb}$ contributions to this term, indicates that this value is almost entirely due to $\Delta Q^{A''}_{Orb}$ ensuing to the π N←Pt^{II} back-donation. Moreover, the $\Delta Q^{A'}$ charge result is slightly positive and is in line with the occurrence of both competitive σ/π interactions in this irreducible representation with the predominance of the σ interaction.

The effect of the bond formation on the CN group is also mirrored in the behavior of the C_{CN}, which in all cases experiences a small electron density depletion. Concerning the $PtCl_2$ moiety, Pt experiences an electronic density depletion (positive Δ*Q* charge), due to the N–Pt^{II} bond formation (slightly higher for ***cis*-1**). This behavior has a twofold origin: (i) the N←Pt^{II} π back-donation contribution in A″ (negative $\Delta Q^{A''}_{Orb}$ charge on N), partially compensated by the predominant N→Pt^{II} σ interaction in A′ (positive $\Delta Q^{A'}_{Orb}$ charge on N), and (ii) the presence of the halogens, the latter acting differently for ***cis*-1** and ***trans*-1**. For ***cis*-1**, in both coordination steps, two different negative Δ*Q* values were obtained for the halogens, depending on the *cis* or *trans* position of the incoming ligand.

For ***cis*-1** and ***trans*-1** the $\Delta Q^{A'}_{Pauli}$ terms are very similar in all coordination steps, indicating that the orbitals' polarization contribution is the same for all halogens regardless of the *cis*/*trans* configuration of the incoming ligand. In addition, by the σ N→Pt→Cl interaction in the *trans* configuration, which brings to a higher electronic density along the *trans* N–Pt–Cl

Table 3 Voronoi Δ*Q* (e^-) and ΔQ^{Γ} contributions for the Pt–L bond formation for ***cis*-1** and ***trans*-1** complexes. Pauli ($\Delta Q^{\Gamma}_{Pauli}$) and orbitals' ($\Delta Q^{\Gamma}_{Orb}$) contributions are given in parentheses. (Data for ***cis*-/*trans*-2**, ***cis*-/*trans*-3**, ***cis*-/*trans*-4**, ***cis*-/*trans*-5**, complexes are given in Tables S2–S5 as the ESI‡)

	***cis*-1**						***trans*-1**			
	S1			**S2**			**S2**			
	Δ*Q* TOT	ΔQ^{Γ} ($\Delta Q^{\Gamma}_{Pauli}$; ΔQ^{Γ}_{Orb}) A′	A″	Δ*Q* TOT	ΔQ^{Γ} ($\Delta Q^{\Gamma}_{Pauli}$; ΔQ^{Γ}_{Orb}) A′	A″	Δ*Q* TOT	ΔQ^{Γ} ($\Delta Q^{\Gamma}_{Pauli}$; ΔQ^{Γ}_{Orb}) A′	A″
Pt	0.14	0.06 (0.05; 0.001)	0.08 (−0.01; 0.007)	0.14	0.07 (0.06; 0.01)	0.07 (−0.01; 0.08)	0.10	0.04 (0.06; −0.02)	0.06 (−0.01; 0.07)
Cl	-0.05^{C}	-0.05^{C} (−0.03; −0.02)	0.00^{C} (0.00; 0.00)	-0.06^{C}	-0.07^{C} (−0.04; −0.03)	0.01^{C} (0.00; 0.01)	−0.05	−0.06 (0.03; −0.09)	0.01 (0.00; 0.01)
	-0.13^{T}	-0.15^{T} (−0.05; −0.10)	0.02^{T} (0.00; 0.02)	-0.14^{T}	-0.17^{T} (−0.04; −0.13)	0.03^{T} (0.00; 0.03)			
N	−0.05	0.06 (0.04; 0.02)	−0.11 (0.01; −0.12)	-0.01^{S2}	0.09^{S2} (0.05; 0.04)	-0.10^{S2} (0.02; −0.12)	-0.04^{S2}	0.07^{S2} (0.03; 0.04)	-0.11^{S2} (0.01; −0.12)
				0.02^{S1}	0.01^{S1} (0.00; 0.01)	0.01^{S1} (0.00; 0.01)	-0.03^{S1}	-0.05^{S1} (−0.02; −0.03)	0.02^{S1} (0.00; 0.02)
C_N	0.05	0.05 (−0.02; 0.07)	0.00 (−0.01; 0.01)	0.04^{S2}	0.05^{S2} (−0.02; 0.07)	-0.01^{S2} (−0.01; 0.00)	0.07^{S1}	0.05^{S2} (−0.02; −0.07)	0.02^{S2} (0.00; 0.02)
				-0.01^{S1}	0.00^{S1} (0.00; 0.00)	-0.01^{S1} (0.00; −0.01)	-0.02^{S2}	-0.02^{S1} (−0.02; 0.00)	0.00^{S1} (0.00; 0.00)

[a] The italic ^{C,T} superscripts are referred to the *cis*/*trans* position of the incoming ligand, respectively. [b] **S1**, **S2** superscripts are referred to the atoms bonded in **S1** and **S2**, respectively.

bond and the ensuing polarization of the Pt–Cl bond towards the more electronegative chlorine atoms.

For ***trans*-1** where all halogens are in *cis* with respect to the incoming ligands, the $\Delta Q^{A'}_{Orb}$ term is slightly higher with respect to the analogous configuration in ***cis*-1** ascribable to the lack of the strongest interaction in *trans*.

The trend of the halogen charges seems to well agree with the *cis*/*trans* influence of the incoming ligand on the Pt–Cl bond length. Indeed, with respect to the relaxed $^{C,T}PtCl_2$ fragments, in ***cis*-1** and ***trans*-1** the Pt–Cl distances result in an elongation of about 0.12 Å and 0.17 Å, respectively, after coordination. For ***trans*-1**, only the *cis* influence is considered, while for ***cis*-1** both effects occur, from which is inferred a higher *cis* influence of the ligand, *i.e.*, the lower Pt/Cl charge depletion/increase in ***trans*-1** with respect to ***cis*-1**. To note are the similar ΔQ values for the chlorines in *cis* both in ***cis*-1** and in ***trans*-1**.

EDA-NOCV analysis

EDA-NOCV analysis allowed a quantitative evaluation of the energies concerning the bonding mechanisms so far discussed.

The results for ***cis*-1** and ***trans*-1** are given in Table 4, while data for all complexes are reported in Table S6 as the ESI.‡ The outcomes for all *trans* complexes in **S1** are not reported due to the non-Aufbau configuration adopted for $^{T}PtCl_2$, for which it is not possible to discriminate the electronic excitation energy contribution. Also in this case we still summarize the results obtained for ***cis*-1** and ***trans*-1** due to the analogies for all complexes (a more detailed discussion is given in the ESI‡).

Concerning ΔE_{Strain}, the higher value in **S1** for all mono-coordinated *cis* species, is rooted almost entirely to the distortion of $^{C}PtCl_2$ and corresponds to the energy needed to shrink the ClPtCl angle from *ca.* 129° to 90°, going from the free to the mono-coordinated $^{C}PtCl_2$.

Table 4 EDA-NOCV analysis for all complexes. The coordination STEP1 for *trans*-complexes is not reported due to the non-Aufbau configuration used for the $^{T}PtCl_2$ fragment (see the Computational methods section)

	***cis*-1**		***trans*-1**
Complex	**S1**	**S2**	**S2**
EDA			
ΔE_{Pauli}	141.63	152.33	155.54
ΔE_{Elec}	−112.34	−113.91	−120.76
ΔE_{Orb}	−72.83	−73.44	−82.25
$\Delta E^{\sigma A'}_{Orb}$	−41.08 (56%)[b]	−43.14 (59%)	−48.16 (59%)
$\Delta E^{\pi A'}_{Orb}$	−11.34 (16%)	−9.69 (13%)	−10.55 (13%)
$\Delta E^{\pi A''}_{Orb}$	−12.34 (17%)	−11.81 (16%)	−11.60 (14%)
ΔE_{Disp}	−3.78	−4.55	−5.26
BE	−47.32	−39.56	−52.73
ΔE_{Strain}	9.00	3.01	5.10
ΔE (−DE)[a]	38.32	36.55	47.63

[a] DE = BE + ΔE_{Strain}. [b] % contributions are referred to the total ΔE_{Orb} term.

Moreover, the **S2** data of ***cis*-1** and ***trans*-1** allowed a comparison between the energy contributions of both complexes. The BE and DE for ***trans*-1** showed more stability of about 11–13 kcal mol^{-1}. The explanation of the higher stability of ***trans*-1** resides in the more negative values of the BE due to the higher negative values of the attractive terms (ΔE_{Elec}, and ΔE_{Orb}) while ΔE_{Pauli} was very similar for both complexes. In this case the contribution of the ΔE_{Strain} term does not highly affect the final DE, being only 2.10 kcal mol^{-1} higher for ***trans*-1**.

The final outcomes so far discussed agree with the thermodynamic results. Particularly, by considering the calculated $\Delta H°$ values as corrections to the electronic energies, the DE trend discussed is in accord with the higher stability of ***trans*-1** (analogous results hold for all complexes as reported in the EDA-NOCV discussion in the ESI‡). Finally, EDA-NOCV analysis allowed for singling out the A′ σ and π interactions energies, permitting to quantify the total contribution of the σ and π interactions. The results are given in Table 4 and indicate that the total N←Pt π back-donation represents about 30% of the total ΔE_{Orb} term and ranges from 32% to 37% with respect to the N→Pt σ interaction which means that the orbital interaction is almost entirely characterized (*ca.* 90%) by donor–acceptor interactions (the same results were obtained for all complexes investigated here, see Table S6 in the ESI‡). As already mentioned, the π-acceptor capabilities of the ACN and PhCN ligands in Pt^{II} complexes were qualitatively inferred, even by some of us,[14a] from topological investigations of the electronic density distribution, charge decomposition analysis,[22–24] and composition and overlap intensities of the molecular orbitals involved in the N–Pt^{II} bond.[14a] Bond analysis, and EDA-NOCV results here reported, ultimately assessed the occurrence and the non-negligible contribution of the N←Pt^{II} π interaction.

Infrared properties of the CN bond

A well-known effect arising from the coordination of the RCN ligands upon the Pt^{II} is the observed infrared $\nu_{C\equiv N}$ blue-shift, which is largely used as a tool to confirm the C≡N–Pt^{II} bond formation. Nonetheless, as stated earlier, this behavior has already been experimentally observed, and also confirmed computationally, even for those atoms which do not show π back-donation properties, *e.g.*, alkali and alkaline earth metal ions or H^+, as well.[14,16,18] Moreover, experimental C≡N distances (*r*C≡N) (Table 5) indicate a slight shortening of these distances or at least no elongation of the bond. In general, this behavior appears counterintuitive if considering: (i) the ensuing depletion of electron density along the C_{CN}–N_{CN} axis of the coordinated RCN and, in addition to the systems here investigated, (ii) the N←Pt^{II} π back donation herein assessed involving anti-bonding ligand orbitals, which effects should both to cause a C≡N_d elongation, thus a red-shift. In this context, we calculated the $\nu_{C\equiv N}$ and C≡N force constants ($k_{C\equiv N}$) for the ACN, PhCN, ***cis*-/*trans*-1** and ***cis*-/*trans*-3** complexes as well as for a series of bond paradigms such as $ACNH^+$, $PhCN^+$, and the ACN–BCF_3, and ACN–BCl_3 adducts. In

Table 5 Calculated vibrational frequencies (C≡Nn; cm^{-1}), force constants ($k_{C\equiv N}$; mdyn $Å^{-1}$); distances (rC≡N; Å), of the free and coordinated ACN and PhCN in CH_2Cl_2 solution

	ACN	$ACNH^+$	$ACN–BF_3$	$ACN–BCl_3$	***cis*-1**	***trans*-1**	PhCN	***cis*-3**	***trans*-3**	$PhCNH^+$
$\nu_{C\equiv N}$ [a]										
Calcd[b]	2258	2315	2350 (2302)[c]	2356 (2324)[c]	2306_{as} 2315_{sym}	2317_{as}	2234	2270_{as} 2280_{sym}	2282_{as}	2267
Exptl[d]	2254[14a]	2314[14a]	2376[34]	2380[35]	2330[14a]	2337[14a]	2230[14a]	2286[14a]	2294[14a]	2254[14a]
$k_{C\equiv N}$ [b,e]										
Calcd	17.8	19.7	19.1 (18.0)[c]	18.7 (18.0)[c]	18.1	18.3	17.1	17.3	17.4	18.7
Exptl	17.4[36]	n.d.[f]	18.8[34]	18.7[35]	n.d.	n.d.	n.d.	n.d.	n.d.	n.d.
rC≡N										
Calcd	1.161	1.146	1.152 (1.164)[b]	1.152 (1.161)[b]	1.159	1.155	1.164	1.162	1.159	1.151
Exptl	1.157[36,37]	n.d.	1.135[38]	1.122[38]	1.123[14a]	1.152[14b]	1.158[39]	1.142[14a]	1.141[14a]	n.d.

[a] $\nu_{C\equiv N}$ calculated analytically. [b] Calculated values in CH_2Cl_2 solution for ACN, PhCN, $ACNH^+$, $PhCNH^+$, ***cis*-/*trans*-1** and ***cis*-/*trans*-3** and in vacuum for $ACN–BCF_3$, and $ACN–BCl_3$. [c] Calculated values from ref. 17 at MP2/6-311G(2d,p) level. [d] Experimental values in CH_2Cl_2 solution for ACN, PhCN, $ACNH^+$, $PhCNH^+$, ***cis*-/*trans*-1** and ***cis*-/*trans*-3** and in KBr for $ACN–BCF_3$, and $ACN–BCl_3$. [e] Force constants were calculated from numerical frequencies' calculation. A comparison of the $\nu_{C\equiv N}$ calculated by analytical and numerical methods showed discrepancies no more than 3 cm^{-1}. [f] Not determined.

particular, these included σ acceptors showing N←Pt^{II} π back donation (***cis*-/*trans*-1** and ***cis*-/*trans*-3**), or not ($ACNH^+$, $PhCN^+$, $ACN–BCF_3$, and $ACN–BCl_3$) as well as, concerning $ACNH^+$ and $PhCN^+$, species bearing a positive charge. For the ACN, PhCN, ***cis*-/*trans*-1**, ***cis*-/*trans*-3**, $ACNH^+$ and $PHCN^+$ species, experimental data in CH_2Cl_2 solution were also available.[14] The $\nu_{C\equiv N}$ and $k_{C\equiv N}$ for $ACN–BCF_3$ and $ACN–BCl_3$ were already studied at the MP2/6-31+G(2d,p) level for which the experimental $\nu_{C\equiv N}$ blue-shift was observed and the increase of $k_{C\equiv N}$ after coordination of the ACN was confirmed.[17] The Cartesian coordinates for all models considered were oriented so that the $\nu_{C\equiv N}$ had components only along one axis (z). The results are given in Table 5. The calculated $\nu_{C\equiv N}$ for the coordinated RCN ligands was in good agreement with the experiment showing the expected blue-shift trend, irrespective of the nature of the RCN–X bond.

The calculated $k_{C\equiv N}$ resulted in an increase accordingly. The nature of the bond seemed to generate differences only in the magnitude of the $\nu_{C\equiv N}$ blue-shift.

To elaborate, the purely σ acceptor $ACN–BCX_3$ (X = F, Cl) showed both a higher $\nu_{C\equiv N}$ blue-shift and a $k_{C\equiv N}$ increasing compared to the ***cis*-/*trans*-1** series, characterized by N→Pt σ and N←Pt π interactions, even if the series show a similar $C\equiv N_d$ decrease with respect to the free ligand. To summarize, the formation of the RCN–X species, irrespective of the bonding mechanism, induces a slight shortening of the rC≡N_d, or at least no elongation, which should arise from a strengthening of the C≡N bond and in turn will cause the $\nu_{C\equiv N}$ blue-shift.

In order to get more insights into this behavior we performed an EDA-NOCV analysis of the RC≡NY bond (R = CH_3, Ph; Y = H^+, BF_3, BCl_3, $PtCl_2ACN$, $PtCl_2PhCN$) bond in the free and coordinated ligands by considering suitable RC and NY fragments. The electronic configuration of the fragments was prepared by considering single occupied $2p_{x^1}$, $2p_{y^1}$ and $2p_{z^1}$ (or $2sp_{z^1}$) orbitals for the interacting C_{CN} and N_{CN} atoms. Finally, the analysis was performed both in vacuum and in CH_2Cl_2, the latter only for ACN, PhCN, ***cis*-/*trans*-1**, ***cis*-/*trans*-3**, $ACNH^+$ and $PHCN^+$ species. The results are given in Table S7 as the ESI.‡ Two different trends for the neutral positively charged species were observed with respect to the free ligands. For the neutral species, there is a systematic decrease of both the ΔE_{Pauli} and the ΔE_{Orb} terms as well as a systematic increase of the attractive ΔE_{Elec} term except for $ACN–BF_3$, most likely due to the strong electron withdrawing effect of the fluorine atoms. This causes lower bonding energies (BE) of the neutral RCN–X species with respect to free ligands ones even if we did not observe computationally any rC≡N elongation. The decrease of the attractive ΔE_{Orb} term plays a leading role in the lowering of the BEs which is partially compensated only by the variation of the other two, *i.e.*, ΔE_{Pauli} and the ΔE_{Elec}. Moreover, the lowest π ΔE_{Orb} contributions obtained for ***cis*-/*trans*-1** and for ***cis*-/*trans*-3** match well with the occurrence of the N←Pt^{II} π back-donation.

Concerning the positively charged species, both attractive ΔE_{Elec} and repulsive ΔE_{Pauli} terms showed a decreasing trend while the attractive ΔE_{Orb} increased. In this case, an increase of the BEs with respect to the free ligands was observed.

These results indicate that the $\nu_{C\equiv N}$ blue-shift in these complexes is not correlated to the C≡N bond strength, in agreement with what is already reported for some $Pt(^{II,IV})$–N systems, including the herein investigated ***trans*-1**.[24]

Further information is provided by the deformation density $\Delta\rho$ associated with the pairwise orbital interactions in the RC≡NY bond. In Fig. 8 and 9 the relevant $\Delta\rho s$ for all ACN derivatives are given with the direction of the charge flow indicated as brown→green ($\Delta\rho s$ for all PhCN derivatives are given in Fig. S4 as the ESI‡). For the purely σ acceptors systems reported in Fig. 8, the N–Y bond (see h, o, and t $\Delta\rho s$) resulted more polarized going from the $ACNH^+$ to $ACNBCl_3$ through the $ACNBF_3$, the last representing an intermediate situation between charged and neutral molecules due to the presence of the strong electron withdrawing fluorine atoms. This trend is reflected in the flow charge on the RC≡NY. In $ACNH^+$ there is a slight charge depletion on the C≡N bond (Fig. 8h) which turns into a gradual charge flow increasing from $ACNBF_3$ to

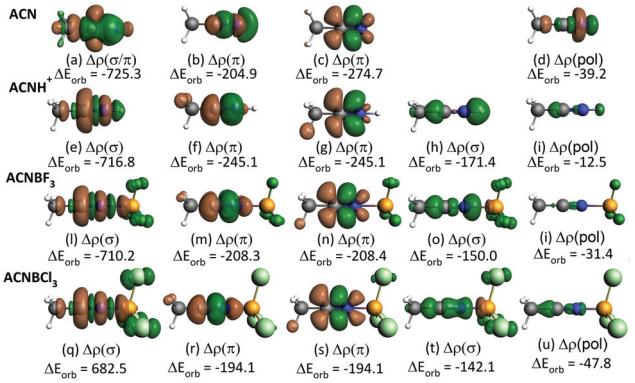

Fig. 8 Plot of the deformation densities $\Delta\rho$ of the pairwise orbitals' interactions and relevant ΔE_{Orb} for the free ACN and related purely σ acceptors' derivatives. Plot isosurfaces 0.003 $e^{1/2}$ $Å^{-3/2}$.

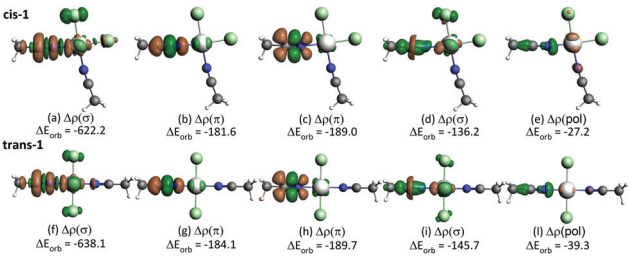

Fig. 9 Plot of the deformation densities $\Delta\rho$ of the pairwise orbitals' interactions and relevant ΔE_{Orb} for ***cis-/trans-*1**. Plot isosurfaces 0.003 $e^{1/2}$ $Å^{-3/2}$.

$ACNBCl_3$ (Fig. 8o and t). This accounts for the small ΔE_{Elec} term in $ACNH^+$ which tends to increase from $ACNBF_3$ up to $ACNBCl_3$ (see Table S7 in the ESI‡). Interestingly, the remaining deformation densities (Fig. 8d, i, p and u), with small ΔE_{Orb} contributions, show an inversion of the RC≡NY σ bond polarization by an orbital pair. These behaviors are ascribable to the origin of the σ N→X ν_{CN} blue-shift in coordinated nitriles.

Indeed, for coordinated carbonyls, the polarization of the C–O bond has already been proposed as the driving force for the shortening of this bond when a positive charge approaches the carbon atoms,[40] as well as to the origin of the high ν_{CO} blue-shift for OC-$BeCO_3$ even in the presence of π back-donation.[41]

In Fig. 9, $\Delta\rho$s for ***cis-/trans-*1** are reported. We will compare the $\Delta\rho$s of these complexes with the purely σ acceptor $ACNBCl_3$ adduct, which is the closest model due to the occurrence of the Cl and the lack of charged species or the high electronegative fluorine atoms. At variance with $ACNBCl_3$, (i) the terms in Fig. 9(d and i) (which are analogous to the term in Fig. 8t) show a charge depletion along the RC≡NY σ bond and (ii) the polarization terms in Fig. 9(e and l) show the lack of the N charge increasing along the C≡N bond when compared to the analogous term in Fig. 8u.

A clearer picture of the effect of the C≡N polarization is attained by inspection of the corresponding VDD charges for

Table 6 Calculated C_{CN} and N_{CN} VDD charges (e^-) (ΔQ) and C≡N charge separation ($\Delta\Delta Q$(C–N))

Compound	$\Delta Q(C_{CN})$	$\Delta Q(N_{CN})$	$\Delta\Delta Q$(C–N)
ACN	−0.04	−0.05	−0.01
$ACNH^+$	+0.28	−0.31	0.59
$ACNBF_3$	+0.25	−0.10	0.35
$ACNCl_3$	+0.33	+0.05	0.28
***cis*-1**	+0.32	+0.19	0.13
***trans*-1**	+0.34	+0.18	0.16
PhCN	+0.20	−0.19	0.39
$PhCNH^+$	+0.23	−0.35	0.58
***cis*-1**	+0.32	+0.18	0.14
***trans*-1**	+0.35	+0.22	0.13

C_{CN} and N_{CN} reported in Table 6. Negative charges on the N_{CN} atom, in the coordinated ligands, were obtained for the protonated (the more negative ones) and $ACNBF_3$ species, while the highest electron density depletion, as previously discussed, was observed for the N atom in the platinum complexes.

Note that the C_{CN} atoms experience a charge depletion in all complexes, with the smallest positive charges observed for the $ACNBF_3$ species. Conversely to N_{CN}, for neutral species, C_{CN} shows similar ΔQ values. Thus, the highest positive N_{CN} ΔQ values obtained for ***cis-/trans-*(1,3)** complexes are ascribable to the contribution of the N←Pt π back-donation, which involves CN* orbitals, which causes an electron density depletion on the nitrogen atom.

The inspection of Tables 5 and 6 allows for correlating the strength of the $k_{C\equiv N}$ with the $\Delta Q(N_{CN})$ and the $\Delta\Delta Q$(C–N) charge separation trends. Indeed, more negative $\Delta Q(N_{CN})$ values and a higher $\Delta\Delta Q$(C–N) correspond to stronger force constants, *i.e.*, the higher the inversed CN bond polarization is observed the higher force constants are obtained.

Conclusions

The N–Pt^{II} bond has been deeply investigated by DFT methods for a series of organonitrile–$PtCl_2$ complexes of the *cis-/trans-*$(RCN)_2PtCl_2$ kind [RCN (R = Me, CF_3, Ph, CH_3Ph, CF_3Ph)]. The role of the R group resulted almost negligible in the N–Pt bonding mechanism as inferred from thermodynamics. The results showed that the nature of the N–Pt bond is characterized both by the N→Pt^{II} and by the N←Pt^{II} π back-donation interactions, the latter involving virtual anti-bonding π* orbitals of the RCN ligands. VDD charges, and EDA-NOCV analysis further confirmed the occurrence of the N→Pt^{II} π back-donation and that its contribution corresponds to about 30–40% of the total bonding interaction.

These results ruled out the lack, or the occurrence of a negligible as well,[14a,22–24] of any N←Pt^{II} π back-donation associated with the experimental $\nu_{C\equiv N}$ blue-shift observed after coordination of a RCN ligand to $^{C,T}PtCl_2$. In this context, EDA-NOCV further confirmed that the $\nu_{C\equiv N}$ was not correlated to the C≡N bond strength as already previously found.[24] Moreover, an analysis of the deformation density of the inter-

acting pairwise orbitals forming the C≡N bond, showed the occurrence of an inversion of the polarization of the CN bond with respect to the free ligands. It caused an increase of the force constants in accordance with the increase of the CN charge separation. Finally, the effect of the N←Pt^{II} π back-donation, regarding the decrease of the force constants, is explained by the loss of the electron population on the nitrogen which leads to the smallest CN charge separation. The N←Pt^{II} π back-donation cannot overcome the σ $\nu_{C\equiv N}$ blue-shift causing only a lowering of this value.

Computational details

All DFT calculations were carried out by using the ADF package (v. ADF 2013.01).[42–44]

Geometries' optimizations

Optimizations of geometries were performed by taking full advantage of the symmetry, namely C_s, at the ZORA[45–48] relativistic scalar level, by adopting the robust GGA functional BP86[49–51] and the D3(BJ) dispersion correction,[52,53] in conjunction with all-electron triple-ζ, doubly polarized, Slater type basis sets,[54] (TZ2P), for all but one atom. All-electron quadruple-ζ, with four polarization functions, (QZ4P), were adopted for F. All optimized structures were confirmed to be a minimum through an evaluation of their harmonic vibrational frequencies. The use of the QZ4P basis set for F was needed to obtain all real harmonic vibrational frequencies for complexes containing this element. The systems herein considered were considered as isolated molecules because we focused on the intra-molecular contributions to the bond properties (optimized coordinates for all complexes are given in Tables S8 and S9 of the ESI‡). Finally, the effectiveness of the optimization protocol was checked by comparing selected geometrical parameters pertaining to ***cis*-1**, ***cis*-2**, ***trans*-2** complexes, for which crystallographic data were recently revised and reported by some of us,[14a] and ***trans*-1**.[14b] The calculated geometrical parameters were in very good agreement with the experimental data (see Table S10 in the ESI‡).

Thermochemistry

Thermochemistry calculations were carried out according to Scheme (a) by using the approach described elsewhere.[21,55,56]

$$^{C,T}PtCl_2 + 2L \rightarrow {}^{C,T}PtCl_2L_2 \quad (a)$$

In particular, gas phase ΔH° values, at 298.15 K and 1 atm, were obtained from analytical frequencies' calculations as correction to the electronic energy and assuming an ideal behaviour:

$$\Delta H^\circ = \Delta E_e + \Delta E_{t(298)} + \Delta E_{r(298)} + \Delta E_{v(0)} + E_{v(0;298)} + \Delta(pV) \quad (1)$$

where ΔE_e is the electronic bonding energy difference between the products and the reactants:

$$\Delta E_e = E_{e\_cpx} - [(E_{e\_trans PtCl_2}) + (2 \times E_{e\_L})] \quad (1a)$$

while E_{e_cpx} is the energy of the complex, $E_{e\_trans PtCl_2}$ is the energy of the $^{T}PtCl_2$ fragment, and E_{e_L} is the energy of the corresponding ligand. $^{T}PtCl_2$ was slightly more stable (*ca.* 3 kcal mol^{-1}) than the $^{C}PtCl_2$ isomer, thus it was considered as the reference for the electronic energy of the $PtCl_2$ fragments. This accounts for the energy needed to move from the linear to the bent form of the $PtCl_2$ moiety. Moreover, $\Delta E_{t(298)}$, $\Delta E_{r(298)}$, and $\Delta E_{v(0)}$ are the differences between the reactants and the products in translational, rotational and zero-point vibrational energy, respectively; $\Delta E_{v(0;298)}$ is the change in the vibrational energy going on from 0 to 298.15 K. As far as the molar work term ($\Delta(pV)$) is concerned, it was considered as (Δn)RT, where $\Delta n = -2$ (see Scheme (a)).

Finally, ΔG° was calculated as:

$$\Delta G^\circ = \Delta H^\circ + T\Delta S^\circ \quad (2)$$

A further set of calculations was also performed to calculate ΔG values at 273.15 K.

Bond analysis

Bond analysis was carried out in C_s symmetry, by considering mono- and di-coordinated species, in the canonical KS-MO framework, according to the following schemes:

mono-coordinated: STEP1 $^{C,T}PtCl_2 + L \rightarrow {}^{C,T}PtCl_2L$ (**S1**)

di-coordinated: STEP2 $^{C,T}PtCl_2L + L \rightarrow {}^{C,T}PtCl_2L_2$ (**S2**)

Before moving further, it needs to be emphasized that the $^{T}PtCl_2$ ground state is an open-shell system with two degenerate singly occupied molecular orbitals; namely, the 40a′(↑) and 17a″(↑) MOs (in the C_s subgroup symmetry here used) which correspond to the $5\pi^{-}_{g}$ and $5\pi^{+}_{g}$ orbitals, respectively, in the $D_{\infty h}$ symmetry group to which $^{T}PtCl_2$ belongs. Thus, to avoid any intra-electronic rearrangement in $^{T}PtCl_2$, we needed to "prepare" the fragment by properly setting up its frontier electronic structure by switching from the 15a″37a′38a′16a″39a′40a′(↑)17a″(↑) configuration to the 37a′15a″38a′$^{(0)}$39a′16a″40a′17a″ one.

Energy decomposition analysis – natural orbital for chemical valence (EDA-NOCV)

The interaction energy between the fragments considered, see **S1** and **S2** schemes, was analyzed by considering its decomposition, into interaction (ΔE_{int}) and strain (ΔE_{strain}) energy contributions according to the extended transition state method.[26–29] In agreement with this scheme, the total energy ΔE, may be written as:

$$\Delta E = \Delta E_{Int} + \Delta E_{Strain} \quad (3)$$

$$\Delta E_{int} = \Delta E_{Elec} + \Delta E_{Pauli} + \Delta E_{Orb} + \Delta E_{Disp} \quad (4)$$

where, ΔE_{Elec}, ΔE_{Pauli}, and ΔE_{Orb} represent contributions due to the electrostatic interaction, the Pauli repulsion (hereafter, $\Delta E_{Elec} + \Delta E_{Pauli} = \Delta E_{Ster}$, the steric repulsion), and the orbital interaction, respectively. As far as ΔE_{Disp} is concerned, it represents the contribution due to the dispersion corrections. Incidentally, the ΔE_{Orb} term was further decomposed into the irreducible representations' (irreps) contributions, ΔE^{Γ}_{Orb}.[26–28]

In addition to that, it can be of some interest to point out that ΔE_{Strain} – see eqn (3) – provides information about the energy required to distort the free fragment structures to the geometry they assume in the final complex. Finally, ΔE_{Int} and $-\Delta E$ are defined as bonding (BE) and dissociation (DE) energies, respectively. We did not account for the basis set superposition error due to their very low contribution, less than 1 kcal mol^{-1}, to the bonding energy.[14a] In the EDA-NOCV formalism, the ΔE_{Orb} is expressed in terms of Natural Orbitals for Chemical Valence.[30,31] The orbital interaction is then expressed in terms of a few NOCV pairs, for which it is possible to visualize for each ±k orbitals pair their deformation density $\Delta\rho_{\text{k}}(r)$ as well as the corresponding energy contribution $\Delta E^{\text{k}}_{\text{Orb}}$.

Voronoi deformation density (VDD) analysis

Charge distribution was determined by using the VDD approach to analyze the electron density deformation.[25] According to the VDD scheme, the charge rearrangement was determined as,

$$\Delta Q_{\text{A}} = -\int_{\text{V}} \left(\rho(r) - \sum_i \rho_i(r) \right) \text{d}r \tag{5}$$

where V corresponds to the Voronoi cell of atom A into the molecule, $\rho(r)$ is the electron density of the molecule, and $\sum_i \rho_i(r)$ is the promolecule, used as the reference. Thus, VDD charges represent the electron density flowing from/towards an atom, according to which positive/negative values correspond to the loss/gain of electrons, respectively. This approach allows for taking care of small, subtle charges' redistribution taking place in the interacting fragments.[25,57] ΔQ_{A} values were also decomposed into the $\Delta Q_{\text{Pauli,A}}$ and $\Delta Q_{\text{Orb,A}}$ terms (thus $\Delta Q_{\text{A}} = \Delta Q_{\text{Pauli,A}} + \Delta Q_{\text{Orb,A}}$), which were further split into contributions of the different irreps Γ ($\Delta Q^{\Gamma}_{\text{Pauli,A}}$ and $\Delta Q^{\Gamma}_{\text{Orb,A}}$) to quantify their participation to the final ΔQ_{A} values.

Partial density of states (PDOS) and crystal orbital overlap population (COOP)

PDOS were calculated based on Mulliken's prescription for partitioning the overlap density.[58] Further insights into the bonding/antibonding Pt^{II}–ligand interaction were obtained by evaluating the corresponding COOP.[59]

Abbreviations

ACN	Acetonitrile
PhCN	Benzonitrile
CF_3CN	Trifluoroacetonitrile
p-TOL	*p*-Tolunitrile; (4-methylbenzonitrile)
p-TFM	(Trifluoromethyl)benzonitrile
***cis*-1**	*cis*-$PtCl_2(ACN)_2$
***trans*-1**	*trans*-$PtCl_2(ACN)_2$
***cis*-2**	*cis*-$PtCl_2(CF_3CN)_2$
***trans*-2**	*trans*-$PtCl_2(CF_3CN)_2$
***cis*-3**	*cis*-$PtCl_2(PhCN)_2$
***trans*-3**	*trans*-$PtCl_2(PhCN)_2$
***cis*-4**	*cis*-$PtCl_2(TOL)_2$
***trans*-4**	*trans*-$PtCl_2(TOL)_2$
***cis*-5**	*cis*-$PtCl_2(TFM)_2$
***trans*-5**	*trans*-$PtCl_2(TFM)_2$

Conflicts of interest

There are no conflicts to declare.

Acknowledgements

The Computational Chemistry Community (C3P) of the University of Padova is kindly acknowledged. This work was supported by the University of Padova (grant: P-DISC #CARL-SID17 BIRD2017-UNIPD, project CHIRoN).

Notes and references

1 (*a*) V. Yu. Kukushkin and A. J. L. Pombeiro, *Chem. Rev.*, 2002, **102**, 1771; (*b*) R. A. Michelin, M. Mozzon and R. Bertani, *Coord. Chem. Rev.*, 1996, **147**, 299.
2 N. A. Bokach, M. L. Kuznetsov and V. Y. Kukushkin, *Coord. Chem. Rev.*, 2011, **255**, 2946.
3 N. A. Bokach and V. Yu. Kukushkin, *Russ. Chem. Rev.*, 2005, **74**, 153.
4 F. F. Fleming and Q. Wang, *Chem. Rev.*, 2003, **103**, 2035.
5 F. F. Fleming, L. Yao, P. C. Ravikumar, L. Funk and B. C. Shook, *J. Med. Chem.*, 2010, **53**, 7902.
6 (*a*) V. Yu. Kukushkin and A. J. L. Pombeiro, *Inorg. Chim. Acta*, 2005, **358**, 1; (*b*) M. L. Kuznetsov, 2002, **71**, 265. Q13
7 M. L. Kuznetsov, N. A. Bokach, V. Yu. Kukushkin, T. Pakkanen, G. Wagner and A. J. L. Pombeiro, *J. Chem. Soc., Dalton Trans.*, 2000, **24**, 4683.
8 M. L. Kuznetsov, V. Yu. Kukushkin, M. Haukka and A. J. L. Pombeiro, *Inorg. Chim. Acta*, 2003, **356**, 85.
9 M. L. Kuznetsov, N. A. Bokach, V. Yu. Kukushkin and A. I. Dementev, *Russ. J. Gen. Chem.*, 2009, **79**, 232.
10 M. L. Kuznetsov and V. Yu. Kukushkin, *Molecules*, 2017, **22**, 1141.
11 A. S. Kritchenkov, N. A. Bokach, M. L. Kuznetsov, F. M. Dolgushin, T. Q. Tung, A. P. Molchanov and V. Yu. Kukushkin, *Organometallics*, 2012, **31**, 687.
12 D. Fraccarollo, R. Bertani, M. Mozzon, U. Belluco and R. A. Michelin, *Inorg. Chim. Acta*, 1992, **201**, 15.
13 F. D. Rochon, R. Melanson, H. E. Howard-Lock, C. J. L. Lock and G. Turner, *Can. J. Chem.*, 1984, **62**, 860.
14 (*a*) R. Bertani, M. Mozzon, P. Sgarbossa, S. Tamburini, M. Casarin, G. Mangione, G. Casella, A. Venzo, S. Rizzato and A. Albinati, *Inorg. Chim. Acta*, 2017, **455**, 489; (*b*) J. Kritzenberger, H. Yersin, K.-J. Range and M. Zabel, *Z. Naturforsch., B: Chem. Sci.*, 1994, **49**, 297.

15 K. F. Purcell and R. S. Drago, *J. Am. Chem. Soc.*, 1966, **88**, 919.
16 Y. Dimitrova, *J. Mol. Struct. (THEOCHEM)*, 1995, **343**, 25.
17 H.-G. Cho and B.-S. Cheong, *J. Mol. Struct. (THEOCHEM)*, 2000, **496**, 185.
18 J. Reedijk, A. P. Zuur and W. L. Groeneveld, *Recl. Trav. Chim. Pays-Bas*, 1967, **86**, 1127.
19 M. L. Kuznetsov and A. J. L. Pombeiro, *Dalton Trans.*, 2003, 738.
Q14
20 L. P. Wolters and F. M. Bickelhaupt, *ChemistryOpen*, 2013, **2**, 106.
21 J. Nitsch, L. P. Wolters, C. Fonseca Guerra, F. M. Bickelhaupt and A. Steffen, *Chem. – Eur. J.*, 2017, **23**, 614.
22 M. L. Kuznetsov, A. I. Dement'ev, O. S. Shestakova and V. Yu. Kukushkin, *Russ. J. Inorg. Chem.*, 2001, **46**, 1528.
23 M. L. Kuznetsov, *J. Mol. Struct. (THEOCHEM)*, 2004, **674**, 33.
24 M. L. Kuznetsov, A. I. Dement'ev and A. A. Nazarov, *Russ. J. Inorg. Chem.*, 2005, **50**, 731.
25 C. Fonseca Guerra, J.-W. Handgraaf, E. J. Baerends and F. M. Bickelhaupt, *J. Comput. Chem.*, 2004, **25**, 189.
26 T. Ziegler and A. Rauk, *Theor. Chim. Acta*, 1977, **46**, 1.
27 T. Ziegler and A. Rauk, *Inorg. Chem.*, 1979, **18**, 1558.
28 T. Ziegler and A. Rauk, *Inorg. Chem.*, 1979, **18**, 1755.
29 K. Morokuma, *Acc. Chem. Res.*, 1977, **10**, 294.
30 M. Mitoraj, A. Michalak and T. Ziegler, *J. Chem. Theory Comput.*, 2009, **5**, 962.
31 M. Mitoraj, A. Michalak and T. Ziegler, *Organometallics*, 2009, **28**, 3727.
32 R. A. Sustmann, *Tetrahedron Lett.*, 1971, **12**, 2717.
33 R. A. Sustmann, *Tetrahedron Lett.*, 1971, **12**, 2721.
34 B. Swanson and D. F. Shriver, *Inorg. Chem.*, 1970, **9**, 1406.
35 D. F. Shriver and B. Swanson, *Inorg. Chem.*, 1971, **10**, 1354.
36 G. Herzberg, *Electronic Spectra and Electronic Structure of Polyatomic Molecules*, Van Nostrand, New York, 1966.
37 J. L. Duncan, D. C. Mckean and N. D. Michie, *J. Mol. Struct.*, 1974, **21**, 405.
38 B. Swanson, D. F. Shriver and J. A. Ibers, *Inorg. Chem.*, 1969, **8**, 2182.
39 J. Casado, L. Nygaard and G. O. Sørensen, *J. Mol. Struct.*, 1971, **8**(1), 211–224.
40 (*a*) A. J. Lupinetti, S. Fau, G. Frenking and S. H. Strauss, *J. Phys. Chem. A*, 1997, **101**, 9551; (*b*) A. S. Goldman and K. Krogh-Jespersen, *J. Am. Chem. Soc.*, 1996, **G118G**, 12159.
41 M. Chen, Q. Zhang, M. Zhou, D. M. Andrada and G. Frenking, *Angew. Chem., Int. Ed.*, 2015, **54**, 124.
42 G. te Velde, F. M. Bickelhaupt, E. J. Baerends, C. Fonseca Guerra, S. J. A. van Gisbergen, J. G. Snijders and T. Ziegler, *J. Comput. Chem.*, 2001, **22**, 931.
43 C. Fonseca Guerra, J. G. Snijders, G. te Velde and E. J. Baerends, *Theor. Chem. Acc.*, 1998, **99**, 391.
44 *ADF2013, SCM*, Theoretical Chemistry, Vrije Universiteit, Amsterdam, The Netherlands, http://www.scm.com.
45 E. van Lenthe, E. J. van Baerends and J. G. Snijders, *J. Chem. Phys.*, 1993, **99**, 4597.
46 E. van Lenthe, E. J. Baerends and J. G. Snijders, *J. Chem. Phys.*, 1994, **101**, 9783.
47 E. van Lenthe, R. van Leeuwen, E. J. Baerends and J. G. Snijders, *Int. J. Quantum Chem.*, 1996, **57**, 281.
48 E. van Lenthe, A. Ehlers and E. J. Baerends, *J. Chem. Phys.*, 1999, **110**, 8943.
49 A. D. Becke, *Phys. Rev. A*, 1988, **38**, 3098.
50 J. P. Perdew, *Phys. Rev. B: Condens. Matter Mater. Phys.*, 1986, **33**, 8822.
51 J. P. Perdew, *Phys. Rev. B: Condens. Matter Mater. Phys.*, 1986, **34**, 7406.
52 S. Grimme, *J. Comput. Chem.*, 2004, **25**, 1463.
53 S. Grimme, S. Ehrlich and L. Goerigk, *J. Comput. Chem.*, 2011, **32**, 1456.
54 E. van Lenthe and E. J. Baerends, *J. Comput. Chem.*, 2003, **24**, 1142.
55 M. Swart and F. M. Bickelhaupt, *J. Chem. Theory Comput.*, 2006, **2**, 281.
56 M. Swart, E. Rösler and F. M. Bickelhaupt, *J. Comput. Chem.*, 2006, **27**, 1486.
57 L. Guillaumes, S. Simon and C. Fonseca Guerra, *ChemistryOpen*, 2015, **4**, 318.
58 R. S. Mulliken, *J. Chem. Phys.*, 1955, **23**, 1833.
59 G. J. Miller, *Angew. Chem., Int. Ed. Engl.*, 1989, **101**, 1570.